THE JOURNAL OF PHYSICAL CHEMISTRY A

Article

Cite This: J. Phys. Chem. A 2019, 123, 10947−10960

pubs.acs.org/JPCA

Revealing Long-Range Substituent Effects in the Laser-Induced Fluorescence and Dispersed Fluorescence Spectra of Jet-Cooled $CH_xF_{3-x}CH_2O$ (x = 1, 2, 3) Radicals

Benedek Koncz,[†] Gábor Bazsó,[†,‡] Md Asmaul Reza,[§] Hamzeh Telfah,[§] Kristóf Hegedüs,[∥] Jinjun Liu,*[,§,⊥] and György Tarczay*[,†,#]

[†]ELTE Eötvös University, Institute of Chemistry, Laboratory of Molecular Spectroscopy, PO Box 32, H-1518 Budapest 112, Hungary

[§]Department of Chemistry, University of Louisville, 2320 South Brook Street, Louisville, Kentucky 40292, United States

[∥]Research Centre for Natural Sciences, Institute of Organic Chemistry, PO Box 286, H-1519 Budapest, Hungary

[⊥]Conn Center for Renewable Energy Research, University of Louisville, 2320 South Brook Street, Louisville, Kentucky 40292, United States

[#]MTA-ELTE Lendület Laboratory Astrochemistry Research Group, PO Box 32, H-1518 Budapest 112, Hungary

Supporting Information

The $\tilde{B}-\tilde{X}$ laser-induced fluorescence (LIF) and dispersed fluorescence (DF) spectra of the atmospherically important β-monofluoro ethoxy (MFEO), β,β-difluoro ethoxy (DFEO), and β,β,β-trifluoro ethoxy (TFEO) radicals were recorded with vibronic resolution under jet-cooled conditions. To simulate the spectra, Franck−Condon factors were obtained from quantum chemical computations carried out at the CAM-B3LYP/6-311++G(d,p) level of theory. The simulations reproduce well both the LIF and DF spectra. Both conformers (G and T) of MFEO and one (G) of the two conformers of DFEO contribute to the LIF spectrum. A comparison between the experimental and calculated spectra confirms the expected long-range field effects of the CH_xF_{3-x} group on electronic transition energies and bond strengths, especially in the excited electronic ($\tilde{B}$) state. Although TFEO has only one conformer, its LIF spectrum is highly congested, which is attributed to the interaction between CO stretch and the $-CF_3$ internal rotation.

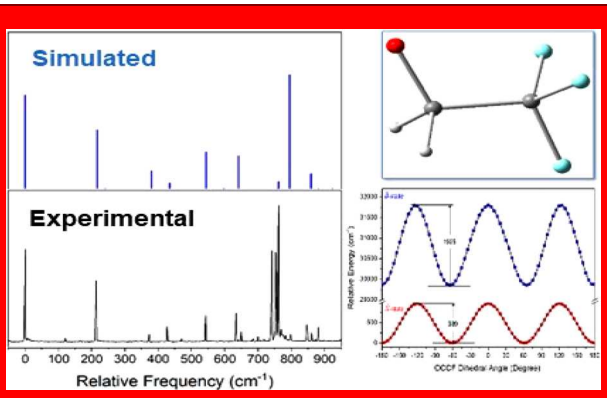

INTRODUCTION

Hydrofluorocarbons (HFCs) are commonly used as refrigerants, solvents, and propellants, and for etching in the semiconductor industry. Their industrial production greatly increased in the late 1980s, because the Montreal Protocol has phased out the production of chlorofluorocarbons (CFCs) that significantly contributed to the depletion of Earth's ozone layer. Although HFCs do not have ozone depletion potential (ODP), it has turned out that these compounds can greatly contribute to global warming. For example, the compounds of monofluoroethane (R161), 1,1-difluoroethane (R152a), and 1,1,1-trifluoroethane (R143a) have zero ODP, while their global warming potentials (GWPs, as compared to CO_2) are 12, 124, and 4470.[1] In addition, each of these compounds is relatively stable in the atmosphere, especially 1,1,1-trifluoroethane, which has an atmospheric lifetime of 40−52 years.[2,3] Realizing this problem, more than 150 nations have agreed in 2016 to cut back their HFC use from 2019. Even if their production would drastically decrease in the next few years, due to their long atmospheric lifetime, HFC pollutants will be present in the atmosphere for decades.

As hydrocarbons, HFCs decompose in the atmosphere by reacting with hydroxyl radical (OH). In the first step of this reaction, a fluorohydrocarbon radical is formed (eq 1), which in subsequent reactions with O_2 and then with NO yields fluorinated alkylperoxy (eq 2) and fluorinated alkoxy radicals (eq 3).[4,5]

$$CH_xF_{3-x}CH_3 + OH \rightarrow CH_xF_{3-x}CH_2 + H_2O \quad (1)$$

$$CH_xF_{3-x}CH_2 + O_2 + M \rightarrow CH_xF_{3-x}CH_2O_2 + M \quad (2)$$

$$CH_xF_{3-x}CH_2O_2 + NO \rightarrow CH_xF_{3-x}CH_2O + NO_2 \quad (3)$$

Therefore, to understand the details of these atmospheric reactions and to monitor these species in the gas phase, first

Received: October 19, 2019
Revised: November 28, 2019
Published: December 2, 2019

DOI: 10.1021/acs.jpca.9b09829
J. Phys. Chem. A 2019, 123, 10947−10960

the structure and the spectra of these species have to be studied and analyzed.

Jet-cooled laser-induced fluorescence (LIF) has been used to study alkoxy radicals in their second excited electronic ($\tilde{B}$) state.[5−24] While moderate-resolution scans provide information on the vibrational levels, high-resolution LIF spectra are suitable to determine experimental rotational and spin-rotational constants. Similarly, dispersed jet-cooled laser-induced fluorescence (DF) spectroscopy has been used to explore the vibrational levels in the ground state ($\tilde{X}$) and in the low-lying first excited electronic ($\tilde{A}$) state,[22,25−28] while stimulated-emission pumping (SEP) and microwave spectroscopy (MW) can provide high enough resolution to obtain rotational constants in the electronic ground state.[29−31] In most of these studies, alkyl nitrites (RONO) have been used as precursors, and the alkoxy radicals were produced by laser photolysis typically at 308, 351, or 355 nm. As it has been shown, Cl and Br substituted alkoxy radicals cannot be prepared by this method, because photon absorption results in a HCl or HBr elimination, respectively.[32] In contrast to this, due to the strong C−F bond, fluorinated alkoxy radicals are the major products of the photochemical decompositions of fluorinated alkyl nitrites. Among the fluorinated alkoxy radicals, trifluoromethoxy (CF_3O)[33] and β-monofluoroethoxy (CH_2F-CH_2O),[34] and the unsaturated 1-fluorovinoxy ($CH_2{=}CFO$)[35−38] and *cis*- and *trans*-1,2-difluorovinoxy radicals ($CFH{=}CFO$)[39] were studied by LIF spectroscopy.

The purpose of the present paper is to characterize β-monofluoro- (MFEO), β,β-difluoro- (DFEO), and β,β,β-trifluoroethoxy (TFEO) radicals by moderate-resolution LIF and DF spectroscopy. We also intended to analyze the tendencies in structural and spectroscopic properties as a function of the number of fluorine atoms, which can help us to understand the reactivity and, therefore, the atmospheric lifetime of these species. The paper is organized as follows. After a description of the experimental and computational methods, we analyze the LIF spectra. This is followed by the discussion of the DF spectra obtained by setting the laser wavelength at the $\tilde{B} \leftarrow \tilde{X}$ band origin and some intense vibrationally excited levels. Finally, we discuss the spectroscopic and structural tendencies.

METHODS

Sample Preparation. Fluoroethyl nitrite was prepared from fluoroethanol (15 g, 235 mmol) dissolved in the solution of sodium nitrite (16.1 g, 235 mmol) and 50 mL water. The solution was chilled in an ice bath to 5 °C and 50% sulfuric acid (23 g, ∼120 mmol) was added dropwise. After adding a few drops from the acid solution, a vigorous reaction started and nitrous fumes evolved from the reaction mixture. The solution was stirred for a further 5 min after the addition of the sulfuric acid. Then the lower organic phase was separated using a glass pipet, washed with a few milliliters of chilled brine, and dried over sodium sulfate. The raw product was purified by distillation (boiling point 62−65 °C, 760 mmHg) under a gentle stream of nitrogen gas and stored over anhydrous sodium carbonate. Yield 6.3 g, 67 mmol. Difluoroethyl nitrite was prepared from difluoroethanol (5 g, 61 mmol) dissolved in the solution of sodium nitrite (4.2 g, 61 mmol) and 15 mL water. The solution was chilled on an ice bath to 5 °C, and 50% sulfuric acid (6 g, ∼30 mmol) was added dropwise. The solution was stirred for further 15 min after the addition of the sulfuric acid. Then the lower organic phase was separated using a glass pipet and washed with a few milliliters of chilled brine. The raw product was dried over sodium sulfate and was stored over anhydrous sodium carbonate. Yield 0.5 g, 4.5 mmol.

The trifluoroethyl nitrite was prepared according to a slightly modified method described by Shuping and co-workers.[40] 50% sulfuric acid (23 g, ∼120 mmol) was added dropwise to the vigorously stirred, chilled solution of trifluoroethanol (25 g, 250 mmol), sodium nitrite (17.3 g, 250 mmol), and 50 mL of water. The solution was kept under 5 °C during the addition. A slow nitrogen gas flow was used to carry the evolved nitrous fumes from the reaction mixture. The products were condensed in a dry ice trap and purified by freeze−pump−thaw.

Spectroscopic Measurements. The spectroscopic measurements were carried out at Eötvös University, Budapest. For LIF and DF investigations, the precursor was placed into a cooled (−20 °C for monofluoroethyl nitrite, −50 °C for di- and trifluoroethyl nitrite) stainless sample holder, and helium flow was passed over the sample at 11 bar. The seeded flow was then expanded through a 300 μm standard pulsed nozzle (General Valve; using 400 μs opening time) into the jet chamber (65 L, cylindrical shape), which was evacuated by a mechanical booster pump backed by a rotary oil pump. To produce the alkoxy radicals, photolysis of the precursors just below the throat of the nozzle was performed using the third harmonic output of a pulsed Nd:YAG (Spectra-Physics Quanta-Ray Lab-150) laser. The photolysis produced the desired fluorinated alkoxy radicals, which were then probed ca. 6−8 mm downstream from the photolysis laser. The probe beam was the frequency-doubled output of a tunable dye laser (Sirah PrecisionScan LG-18) pumped by the second harmonic of a Nd:YAG (Spectra-Physics Quanta-Ray Pro-250) laser at 532 nm. The lasers were operated at 10 Hz. The output of the photolysis laser was 230 mJ per pulse; the estimated photon energy at the molecular beam was 180−200 mJ per pulse. For LIF experiments, <3 mJ energy per pulse was used for excitation, while for DF experiments, the transitions were saturated by 2−6 mJ of excitation energy. Both laser beams were focused by plano-convex 300 and 500 mm focal-length lenses. (Both laser beams were slightly defocused at the point where they crossed the molecular beam.) To cover the total spectral region of the present study, four laser dyes were used: LDS 698 (pyridine 1), DCM, pyrromethane 597, and pyrromethane 597. The delay time between the firing of the photolysis and dye lasers, along with the time delay and the opening time of the nozzle, was controlled by a pulse generator (Quantum Composers 9514). The photolysis and probe beams entered the vacuum chamber through the same window. The fluorescence signal was collected perpendicularly to the laser beams.

On one side of the chamber, the fluorescence emission was collimated by a 1 in. diameter lens (focal length = 33 mm) and a second lens (1 in. diameter, focal length = 75 mm) focused the radiation onto the entrance pinhole (1 mm diameter) of the photomultiplier tube (PMT, Oriel 77348-S) connected to a Tektronix, TPS2024 digital oscilloscope. A 385 nm (for MFEO and DFEO) or a 320 nm (for TFEO) long-pass filter was placed immediately before the PMT to reduce the photon intensity due to the scattering of the photolysis and the excitation laser. The LIF signal was collected by a digital oscilloscope. The scan of the dye laser and data acquisition was controlled by a home-developed LabVIEW program. The step size of the laser-wavelength scan was 0.5 cm^{-1}. At each

DOI: 10.1021/acs.jpca.9b09829
J. Phys. Chem. A 2019, 123, 10947−10960

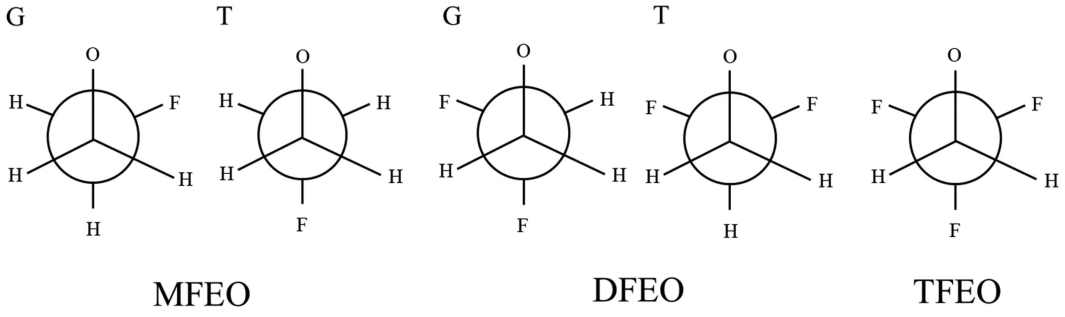

Figure 1. Newman projections of different conformers of the investigated fluoro ethoxy radicals.

Table 1. Geometric Parameters of Different Conformers of Ethoxy, MFEO, DFEO, and TFEO Radicals in the $\tilde{X}$ and $\tilde{B}$ States As Obtained at the CAM-B3LYP/6-311++G(d,p) Level of Theory

		geometric parameter							
		C−O (Å)		∠OCC (deg)		∠CCX[a] (deg)		ϕOCCX[a] (deg)	
isomer	conformer	$\tilde{X}$	$\tilde{B}$	$\tilde{X}$	$\tilde{B}$	$\tilde{X}$	$\tilde{B}$	$\tilde{X}$	$\tilde{B}$
ethoxy		1.36	1.60	116	107	111	106	180	180
MFEO	G	1.36	1.57	115	108	110	113	73	78
	T	1.36	1.57	114	103	109	104	180	180
DFEO	G	1.37	1.55	108	104	114	114	54	51
	T	1.36	1.51	115	107	113	104	180	180
TFEO		1.35	1.53	114	107	110	104	180	180

[a]"X" is the H atom in the C_s plane for ethoxy, F for MFEO, H in the $-CHF_2$ group for DMFE, and the F atom in the C_s plane for TFEO.

wavelength, 16, 32, or 64 laser shots were averaged. The recorded spectra were smoothed by a 5-point Savitzky−Golay method.

On the other side of the chamber, the fluorescence emission was collimated by a 1-in. diameter lens (focal length = 33 mm), and a second lens (diameter = 1 in., focal length = 75 mm) focused the radiation onto the entrance slit of an Acton Spectra Pro 300i monochromator. Two different gratings were used, a 2400 grooves/mm grating (240 nm blaze) for wavelengths shorter than 400 nm and a 1800 grooves/mm grating (500 nm blaze) for wavelengths longer than 400 nm. The detection of the dispersed photons was done with the Princeton Instruments PI-MAX 3 UNGEN II ICCD camera. The entrance slit of the monochromator was set to 200 μm for MFEO radical and 90 μm for TFEO radical. These resulted in ca. 12−19 cm^{-1} and 6−15 cm^{-1} instrumental resolution, respectively, depending on the spectral window and the grating. For DFEO radical 200 μm slit was used for the less intense origin band and 90 μm slit for the other transitions. In most of the cases (except for the TFEO radicals and the low-wavenumber side of some spectra of MFEO and DFEO), the spectral line widths were larger than the instrumental resolution. The DF spectra were calibrated by the laser frequencies. The gate time of the camera was 1000 ns, 1000 laser shots on-chip accumulations were read, and 30 images were summed up. The band origins were recorded with slightly delayed gates to minimize the scattered laser intensity. To obtain a similar signal-to-noise ratio for this window, 40−75 images were accumulated. Each DF spectrum consists of 6−8 spectral windows, each covering 18−25 nm, depending on the grating and the central wavelength. The spectral windows were overlapped, and the intensities were scaled to each other to exclude the effect of the change of fluorescence intensity in time. The spectra were corrected to reduce the background noise, for which a background spectrum was collected with a 0 s long gate applied on the camera (i.e., the amplifier was turned off). Finally, the intensities were scaled by the efficiency curves of the gratings, the spikes (single pixels) due to cosmic rays were removed, and the spectra were smoothed by taking a moving average of 5 data points in the logarithmic representation.

Quantum Chemical Computations. Density functional theory (DFT) computations have been performed to predict geometries, electronic transition frequencies, and vibrational frequencies of the radicals. Computations on the $\tilde{X}$ state were done with the Coulomb-attenuating method (CAM)[41] at the B3LYP/6-311++G(d,p) level of theory, while time-dependent (TD-)CAM-B3LYP/6-311++G(d,p) method was used for the $\tilde{B}$ state. For molecules with C_s symmetry (T conformers), computations of the $\tilde{A}$ state were also carried out by promoting an electron from its HOMO ($2p\pi_y$ localized on the O atom) to LUMO ($2p\pi_x$). All computations were carried out using the Gaussian 09 software package.[42] CAM computations include long-range corrections and hence provided more accurate results that better reproduce the LIF and DF spectra of the investigated free radicals than normal DFT computations (*vide infra*).

Both MFEO and DFEO have two stable conformations distinguished by different OCCF and OCCH dihedral angles. In the present work, the conformers of MFEO and DFEO are defined using ϕOCCF and ϕOCCH, respectively. Following conventions, conformers with approximately ±60° and 180° dihedral angles are referred to in the present work as G and T conformers, respectively (see Figure 1 for molecular Newman projections). TFEO has only one stable conformer. The optimized values of the most important geometric parameters, including the CO bond length, the OCC angle, and the OCCF or OCCH dihedral angles, for both the $\tilde{B}$ and $\tilde{X}$ states of all stable conformers, are summarized in Table 1. Of all the geometric parameters, the $\tilde{B} \leftarrow \tilde{X}$ excitation affects the CO bond length most significantly, because the excitation

DOI: 10.1021/acs.jpca.9b09829
J. Phys. Chem. A 2019, 123, 10947−10960

Table 2. Computed Relative Energies of the G and T Conformers of MFEO and DFEO[a]

	conformer	relative energy (cm^{-1}) (comp)	$\Delta E^{\tilde{A}-\tilde{X}}$ (cm^{-1}) (comp)	$\Delta E^{\tilde{B}-\tilde{X}}$ (cm^{-1}) (comp)	$\Delta E^{\tilde{B}-\tilde{X}}$ (cm^{-1}) (expt)	$\Delta E^{\tilde{B}-\tilde{X}}$ scaling factor	$\tilde{\nu}^{\tilde{X}}_{CO}$($cm^{-1}$) (comp)	$\tilde{\nu}^{\tilde{X}}_{CO}$($cm^{-1}$) (expt)	$\tilde{\nu}^{\tilde{X}}_{CO}$scaling factor	$\tilde{\nu}^{\tilde{B}}_{CO}$($cm^{-1}$) (comp)	$\tilde{\nu}^{\tilde{B}}_{CO}$($cm^{-1}$) (expt)	$\nu^{\tilde{B}}_{CO}$scaling factor
ethoxy			411[b]	29181	29948	0.974	1090	1070	0.982	628	603	0.960
MFEO	G	100.3		30587	29869	0.977	1092	1065	0.975	628	604	0.962
	T[c]	0	1014	31467	30520	0.970	1075, 1100	1041, 1072	0.968, 975	734	695	0.947
DFEO	G	0		32396	29183	0.901	1090	1053	0.966	758	603	0.796
	T[c,d]	585.5	1181	31979			1098			645, 869		
TFEO			1681	33449	32506	0.972	1114	1076	0.966	794	756	0.958

[a] $\tilde{A}-\tilde{X}$ separations ($\Delta E^{\tilde{A}-\tilde{X}}$) of ethoxy, C_s(T) conformers of MFEO and DFEO, and TFEO, their computed and experimental adiabatic transition frequencies of the $\tilde{B} \leftarrow \tilde{X}$ transition ($\Delta E^{\tilde{B}-\tilde{X}}$), and their computed and experimental CO-stretch frequencies in the $\tilde{X}$- and $\tilde{B}$ states ($\tilde{\nu}^{\tilde{X}}_{CO}$ and $\tilde{\nu}^{\tilde{B}}_{CO}$). All calculations are on the CAM-B3LYP/6-311++G(d,p) level of theory. Zero-point energies are included in the calculations of $\Delta E^{\tilde{B}-\tilde{X}}$. [b] Compared to experimental value of 364 cm^{-1} [refs 26 and 52] or 355(10) cm^{-1} [ref 53]. [c] The T conformer of $\tilde{X}$ state MFEO and the T conformer of the $\tilde{B}$ state DFEO have two vibrational modes with the CO-stretch character according to calculations. [d] The T conformer of DFEO was not observed in the LIF spectrum.

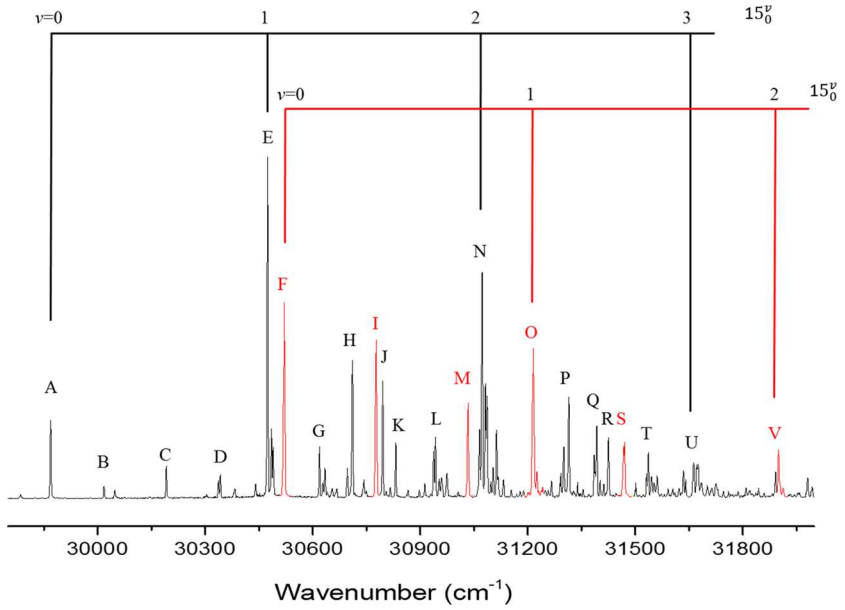

Figure 2. LIF spectrum of jet-cooled MFEO. The strongest vibronic bands are labeled with Latin letters and color-coded for the T (red) and G (black) conformers. Two CO-stretch progressions (15^v_0), belonging to the two conformers, are also denoted.

corresponds to an electron promotion from the 2pσ orbital of the CO bond to the pπ_y orbital localized on the O atom.

Computed relative energies of conformers of each isomer, adiabatic excitation frequencies of their $\tilde{B} \leftarrow \tilde{X}$ transition and the $\tilde{B}$- and $\tilde{X}$-state CO stretch frequencies are listed in Table 2. For conformers with C_s symmetry, that is, T conformers of MFEO and DFEO, as well as TFEO, vibrational modes can be grouped into symmetric (a') and asymmetric (a'') types. In the present paper, all vibrational modes are numbered from high-frequency to low-frequency regardless of symmetry. The calculated frequencies and symmetries (when applicable) are listed in the Supporting Information (Tables S1–S5). Franck–Condon factors (FCFs) for the $\tilde{B} \leftarrow \tilde{X}$ and $\tilde{B} \rightarrow \tilde{X}$ transitions were calculated using the ezSpectrum program.[43] For the $\tilde{B} \leftarrow \tilde{X}$ transitions, a vibrational temperature of 50 K was assumed for calculating the Boltzmann distribution, while for the $\tilde{B} \rightarrow \tilde{X}$ transitions, only those from the ($v' = 0$ level of the $\tilde{B}$ state is included. Due to the large difference in $\tilde{X}$- and $\tilde{B}$-state CO bond length (see Table 1), Duschinsky rotations were taken into account in the calculation of FCFs to better reproduce the experimental spectra.

RESULTS

LIF Spectra. *MFEO.* The survey scan showing the vibronic structure of the $\tilde{B} \leftarrow \tilde{X}$ excitation transition of MFEO is illustrated in Figure 2. The spectrum is very similar to the LIF spectrum of MFEO published by Chhantyal-Pun et al.;[34] the band positions do not differ in the two spectra by more than 2–3 cm^{-1}. The difference is a bit larger when the relative band intensities are compared. The intensity differences can be explained by several factors. First, the different cooling efficiency of the jet expansion (e.g., caused by the different precursor temperature, backing pressure, the pinhole size of the jet, the distance between the photolysis, and the LIF laser, etc.) can result in different rotational band contours and a different ratio of the two conformers. Second, in the present experiment, the flux of the LIF laser was relatively high, in order to identify additional lower intensity bands and extend the spectral region. Although, as it was experimentally checked, it did not cause saturation for the band origin(s), it might have saturated the higher intensity bands as suggested by simulation (*vide infra*).

DOI: 10.1021/acs.jpca.9b09829
J. Phys. Chem. A 2019, 123, 10947–10960

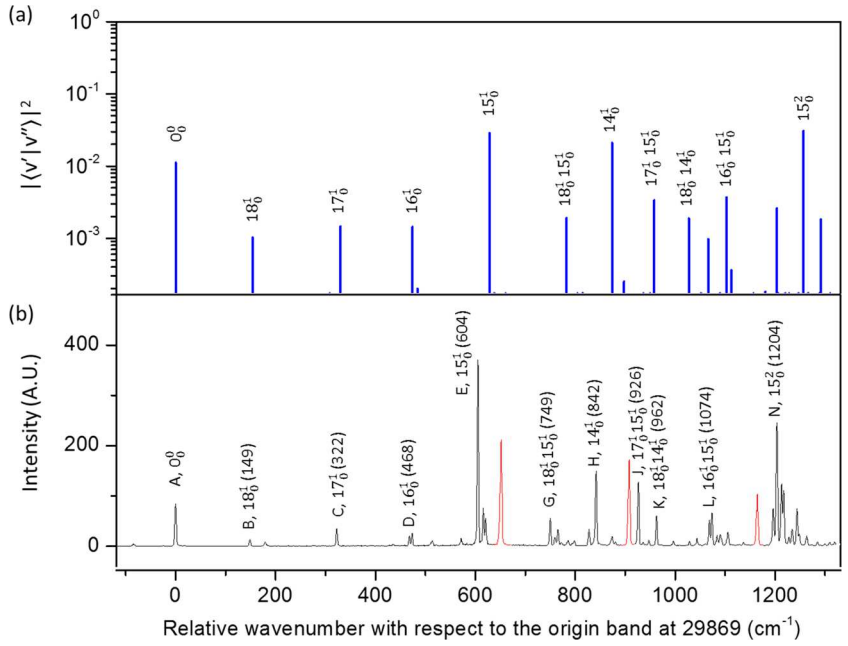

Figure 3. Comparison between the simulated (a) and experimental (b) LIF spectra of the G conformer of the MFEO radical. Numbers in parentheses are transition frequencies relative to the origin band in cm^{-1}.

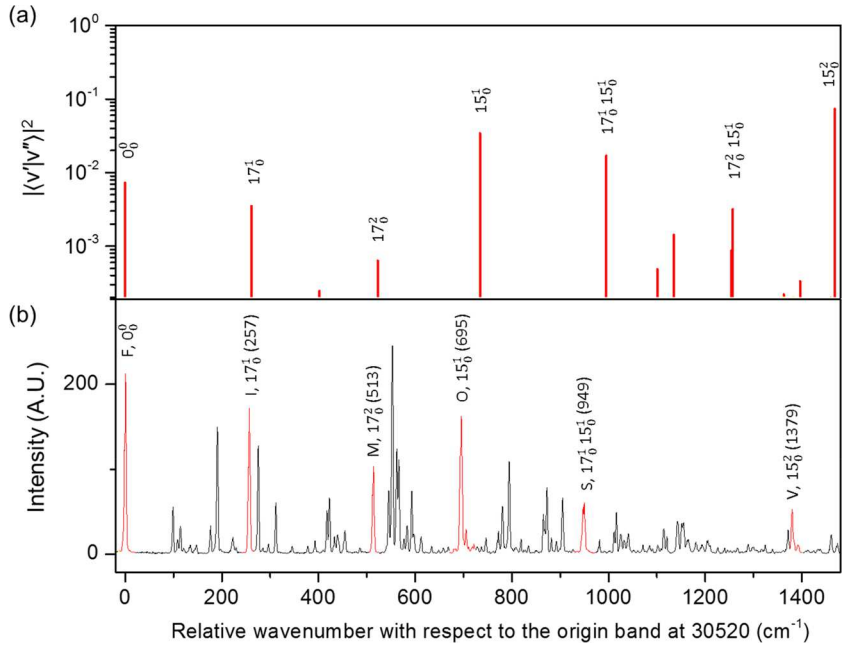

Figure 4. Comparison between the simulated (a) and experimental (b) LIF spectra of the T conformer of the MFEO radical. Numbers in parentheses are transition frequencies relative to the origin band in cm^{-1}.

The strongest vibronic bands are labeled with Latin letters (A through V) in Figure 2. (Note that our labels differ from those of ref 34.) As it was shown by Chhantyal-Pun et al.,[34] the complexity of the spectrum can be explained by the presence of two conformers, G and T. Experimental DF spectra support assigning all observed LIF transitions to two conformers because two types of vibrational structure were observed in DF spectra obtained by pumping different vibronic bands in the LIF spectrum (*vide infra*). The two-conformer assignment is also supported by the computational results. The G conformer is only 100 cm^{-1} higher in energy than the T conformer at the CAM-B3LYP/6-311++G(d,p) level of theory.

In order to check the former assignments and assign more low-intensity bands, the vibronic structure was simulated on the basis of quantum chemical computations and the predicted FCFs. The experimental and the simulated spectra are compared in Figure 3 (for G conformer) and Figure 4 (for T conformer). In agreement with Chhantyal-Pun et al.,[34] the two strong bands at 29869 cm^{-1} (A) and 30520 cm^{-1} (F) were assigned to the G and T conformers, respectively. Our computations overestimate the adiabatic excitation energies by merely ~3%, and the relative order of the two band origins are in agreement with the experiment. They are predicted at

DOI: 10.1021/acs.jpca.9b09829
J. Phys. Chem. A 2019, 123, 10947−10960

Table 3. $\tilde{B} \leftarrow \tilde{X}$ Transition Frequencies (Absolute and Relative to the Origin Bands) And Vibrational Assignments of Strong and Medium Intensity Vibronic Bands Observed in the LIF Spectrum of MFEO[a]

conformer	label	expt freq (cm^{-1})	red shift (cm^{-1})	predicted freq (cm^{-1})	assignment	$\lvert\langle v'\rvert v''\rangle\rvert^2$
G	A	29869	0	0	0^0	0.01119
	B	30018	149	154	18^1[b]	0.00102
	C	30191	322	330	17^1[c]	0.00147
	D	30337	468	474	16^1[d]	0.00145
		30342	473	484	$17^1 18^1$	0.00020
	E	30473	604	628	15^1[e]	0.02865
		30485	616	628	$16^1 18^1$	0.00011
		30489	620	638	$17^1 18^2$	0.00002
	G	30618	749	782	$15^1 18^1$	0.00191
		30634	765	805	$16^1 17^1$	0.00007
	H	30711	842	874	14^1[f]	0.02102
		30742	873	898	13^1[g]	0.00025
	J	30795	926	958	$17^1 15^1$	0.00336
	K	30831	962	1028	$18^1 14^1$	0.00189
		30937	1068	1090	$15^1 18^3$	0.00001
	L	30942	1073	1103	$16^1 15^1$	0.00369
		30953	1084	1112	$15^1 17^1 18^1$	0.00036
	N	31073	1204	1257	15^2	0.03071
		31082	1213	1266	$15^1 17^1 18^2$	0.00003
		31086	1217	1289	$17^2 15^1$	0.00014
		31103	1234	1291	8^1[h]	0.00182
		31113	1244	1311	$10^1 18^1$	0.00008
		31292	1423	1478	5^1[i]	0.00086
		31300	1431	1487	$10^1 17^1$	0.00002
	P	31314	1445	1502	$14^1 15^1$	0.05180
		31339	1470	1526	$13^1 15^1$	0.00071
		31385	1516	1578	$15^1 16^2$	0.00022
	Q	31392	1523	1587	$15^2 17^1$	0.00314
		31402	1533	1622	$8^1 17^1$	0.00028
	R	31424	1555	1656	$16^1 15^1 18^1$	0.00337
		31532	1663	1741	$15^2 17^1 18^1$	0.00024
	T	31536	1667	1747	14^2	0.01796
G		31545	1676	1753	$6^1 17^1$	0.00002
		31552	1683	1766	$8^1 16^1$	0.00025
		31561	1692	1771	$10^1 18^1$	0.00024
		31634	1765	1849	$12^1 15^1 18^1$	0.00006
		31641	1772	1857	$13^1 15^1 17^1$	0.00008
	U	31663	1794	1885	15^3	0.01739
		31673	1804	1900	$14^2 18^1$	0.00159
		31684	1815	1917	$15^2 17^2$	0.00011
		31701	1832	1920	$8^1 15^1$	0.00432
		31713	1844	1940	$12^1 14^1$	0.00150
		31726	1857	1953	$8^1 17^2$	0.00002
		31891	2022	2130	$14^1 15^2$	0.05305
		31981	2112	2215	$15^3 17^1$	0.00147
		31993	2124	2221	$14^2 16^1$	0.00239
T	F	30520	0	0	0^0	0.00728
	I	30777	257	261	17^1[j]	0.00351
	M	31033	513	523	17^2	0.00064
	O	31215	695	734	15^1[k]	0.03430
	S	31469	949	995	$15^1 17^1$	0.01699
				1257	$15^1 17^2$	0.00320
	V	31899	1379	1468	15^2	0.07374

[a]The assignments are based on the calculated $\tilde{B}$ state vibrational frequencies (the 5th column) and FCFs (the last column). Vibrational modes are numbered in descending order. Strong bands are labeled with Latin letters shown in Figure 1. [b]ν_{18}, CH_2O wagging mixed with CH_2F wagging. [c]ν_{17}, OCC bending combined with CCF bending out-of-phase. [d]ν_{16}, OCC bending combined with CCF bending in-phase. [e]ν_{15}, CO stretch. [f]ν_{14}, CC stretch. [g]ν_{13}, CH_2 twist. [h]ν_8, CH_2 rock. [i]ν_5, CH_2 scissor (bending). [j]ν_{17}, OCC bending mode combined with CCF bending in-phase. [k]ν_{15}, CO stretch.

DOI: 10.1021/acs.jpca.9b09829
J. Phys. Chem. A 2019, 123, 10947−10960

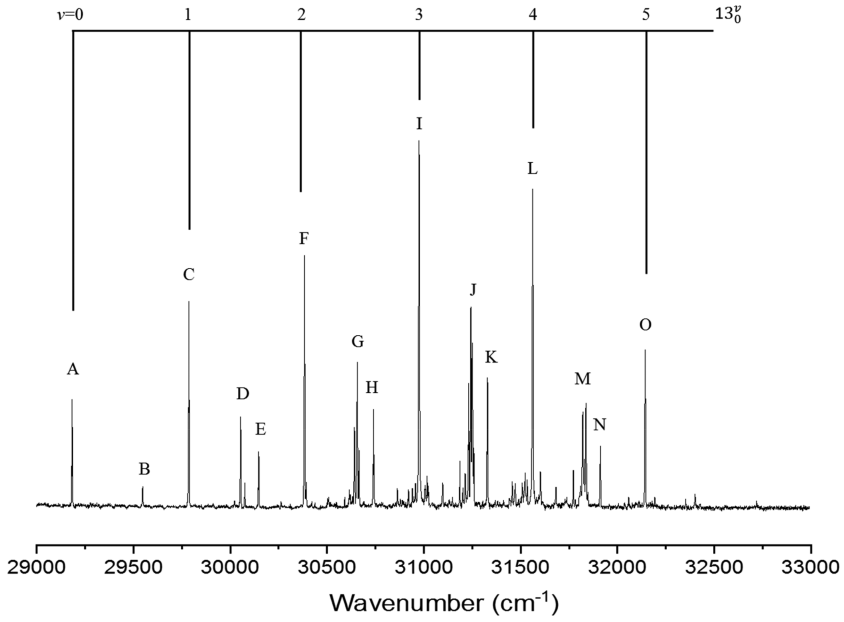

Figure 5. LIF spectrum of jet-cooled DFEO with the CO-stretch progression labeled.

30587 and 31457 cm^{-1} for the G and T conformer, respectively.

The LIF spectrum of MFEO is dominated by two progressions of strong vibronic bands, as indicated in Figure 2. Due to the significant elongation of the CO bond upon the electronic excitation, transitions to the CO-stretch levels are expected to have large FCFs. Therefore, the two strong progressions are assigned to the CO-stretching overtones. Harmonic frequencies and anharmonicity of the CO-stretch mode of both conformers of MFEO have been determined by fitting Birge−Sponer plots (Figures S1 and S2). The fit values are ω_e= 608 cm^{-1}, $\omega_e\chi_e$ = 2 cm^{-1} for the G conformer and ω_e= 706 cm^{-1}, $\omega_e\chi_e$= 6 cm^{-1} for the T conformer. The harmonic frequencies (ω_e) should be compared to the calculated harmonic frequencies of 628 and 734 cm^{-1} for the G and T conformer, respectively (see Table 2).

The predicted vibrational frequencies for the $\tilde{B}$ state of both conformers and the FCFs of vibronic transitions agree well with the experimental ones, and the simulated spectra reproduce well the experimental spectra (Figures 3 and 4). The scaling factor for the $\tilde{B}$-state CO-stretch frequency is 0.962 for the G conformer and 0.947 for the T conformer. It is worth noting that because of the possible saturation of strong bands in the LIF spectrum (*vide supra*), the *y*-axes of the simulated spectra in Figures 3 and 4 are on a logarithmic scale to illustrate the weak vibronic bands.

The experimental frequencies of vibronic bands relative to the origin bands are listed in Table 3 in comparison with the calculated values for both conformers. The assignments, also included in Table 3, are based on the comparison of the LIF spectrum with calculated harmonic vibrational frequencies and FCFs. The LIF spectrum of the G conformer (Figure 3) contains vibronic bands with considerable strength that are assigned to transitions to $\tilde{B}$-state vibrational levels of the CH_2O wagging (ν_{18}), OCC bending combined with CCF-bending out-of-phase (ν_{17}) and in-phase modes (ν_{16}), CO-stretch (ν_{15}), and CC-stretch (ν_{14}) modes, as well as their combination levels. It is expected that these modes have considerable FCFs due to the geometric changes upon the $\tilde{B}$ ← $\tilde{X}$ transition (see Table 1). The vibronic structure of the LIF transition of the T conformer (Figure 4) is significantly simpler compared to that of the G conformer because of its higher symmetry. Only transitions to vibrational levels of the OCC and CCF bending in-phase (ν_{17}) and CO stretch (ν_{15}), as well as their combination levels, are observed.

DFEO. The LIF spectrum of DFEO contains a strong CO-stretch progression starting at 29183 cm^{-1} (band A in Figure 5). The simplicity of the spectrum and the presence of only one strong vibrational progression suggest that all the bands can be assigned to a single conformer. This is in line with our computation, which predicts the energy of the T conformer to be 586 cm^{-1} higher than that of the G conformer. In addition, the computations predict the band origin of the T conformer red-shifted by −417 cm^{-1} with respect to the G conformer. The low-frequency side of the LIF spectrum was extensively scanned, but no additional peaks could be observed. Also, all the bands near the band origin at 29183 cm^{-1} can unambiguously be assigned to conformer G (see Table 4 and Figure 6). Therefore, we can conclude that conformer T has essentially zero population under our jet-cooled conditions.

The experimental vibrational frequencies and their assignments based on the simulation are summarized in Table 4. The consistency between the computed and experimental vibrational frequencies of $\tilde{B}$-state DFEO is somewhat less satisfactory than for MFEO. Most importantly, a strong transition to the vibrational level of OCC bending combined with CCH-bending out-of-phase mode (ν_{17}) is predicted by the simulation. However, this transition is absent in the experimental spectrum (see Figure 6a). Moreover, the computations overestimate the $\tilde{B}$-state frequencies of both the OCC bending combined with CCF bending in-phase mode (ν_{15}) and the CO-stretch mode (ν_{13}). In the former case, the computed frequency is 460 cm^{-1}, while the experimental value is 364 cm^{-1}; therefore, the scaling factor is 0.791 for ν_{15}. For the CO-stretch mode (ν_{13}), the calculated and experimental frequencies are 758 and 603 cm^{-1}, respectively, implying a scaling factor of 0.796. The experimentally determined harmonic frequency of the CO-stretch mode of

DOI: 10.1021/acs.jpca.9b09829
J. Phys. Chem. A 2019, 123, 10947−10960

Table 4. $\tilde{B} \leftarrow \tilde{X}$ Transition Frequencies and Vibrational Assignments of Strong Vibronic Bands Observed in the LIF Spectrum of DFEO[a]

conformer	label	expt freq (cm^{-1})	red shift (cm^{-1})	predicted freq (cm^{-1})	assignment	$\lvert\langle\nu'\rvert\nu''\rangle\rvert^2$
G	A	29183	0	0	0^0	0.02523
				236	17^1[b]	0.00748
	B	29547	364	460	15^1[c]	0.00162
	C	29786	603	758	13^1[d]	0.09288
	D	30053	870	839	$13^1 17^1$	0.02832
	E	30147	964	967	$13^1 15^1$	0.00609
	F	30383	1200	1206	13^2	0.14523
	G	30656	1473	1442	$13^2 17^1$	0.04574
	H	30740	1557	1570	$13^2 15^1$	0.00975
	I	30975	1792	1809	13^3	0.12278
	J	31242	2059	2045	$13^3 17^1$	0.04021
	K	31328	2145	2173	$13^3 15^1$	0.00849
	L	31562	2379	2412	13^4	0.05807
	M	31820	2637	2648	$13^4 17^1$	0.02004
	N	31911	2728	2776	$13^4 15^1$	0.00418
	O	32143	2960	3015	13^5	0.01354

[a]Bands are labeled with Latin letters shown in Figure 4. [b]ν_{17}, OCC bending combined with CCF bending out-of-phase. [c]ν_{15}, OCC bending combined with CCF bending in-phase. [d]ν_{13}, CO stretch.

the G conformer of DFEO is ω_e = 608 cm^{-1} with the anharmonicity $\omega_e\chi_e$= 3 cm^{-1} (see Figure S3). The experimental and simulated LIF spectra of DFEO are compared in Figure 6, in which the two aforementioned scaling factors are applied in generating the simulated spectrum. The simulation with scaled ν_{13} and ν_{15} vibrational frequencies reproduced the experimental spectrum quite well. Vibrational assignments are shown in Figure 6b.

TFEO. The survey scan of the LIF spectrum of TFEO is shown in Figure 7, and the band origin is observed at 32506 cm^{-1}. As expected, the spectrum is dominated by a strong CO-stretch progression. Although TFEO has only one stable conformer, its LIF spectrum is much more congested than that of DFEO. All members of the CO-stretch progression (with the exception of the origin band) and combination bands of the CO-stretch mode are split. Such splitting is attributed to the interaction between CO stretch and the $-CF_3$ internal rotation (see Discussion). Again, assignments are based on the computed $\tilde{B}$ state harmonic vibrational frequencies and FCFs, as summarized in Table 5. As in the case of MFEO, the simulation reproduces well the experimental spectrum (see Figure 8) except that splitting in overtone and combination transitions that involve the CO-stretch mode is not reproduced. For these transitions, the experimental vibronic transition frequencies are calculated as intensity-weighted averages (centers-of-gravity) of transition frequencies of different components of the splitting. The $\tilde{B}$ state fundamental frequency of the CO-stretch mode so determined is 756 cm^{-1}, and the scaling factor for the calculated value is 0.966. The experimentally determined ω_e and $\omega_e\chi_e$ values for the CO-stretch mode of TFEO are 765 and 4 cm^{-1}, respectively (see Figure S4).

DF Spectra. DF spectra obtained by pumping the origin bands in the LIF spectra are presented in Figure 9 (G and T conformers of MFEO), Figure 10 (DFEO), and Figure 11 (TFEO) in comparison with simulation using $\tilde{X}$ state vibrational frequencies and $\tilde{B} \rightarrow \tilde{X}$ transition FCFs. In all cases, the DF spectra are dominated by strong CO-stretch progressions.

The calculations slightly overestimate the frequencies of the CO-stretch mode as well as other vibrational modes. A scaling factor of ~0.97 for the CO-stretch mode (see Table 2) was determined by comparing the calculated CO-stretch frequency to the experimental ones. It is worth pointing out that,

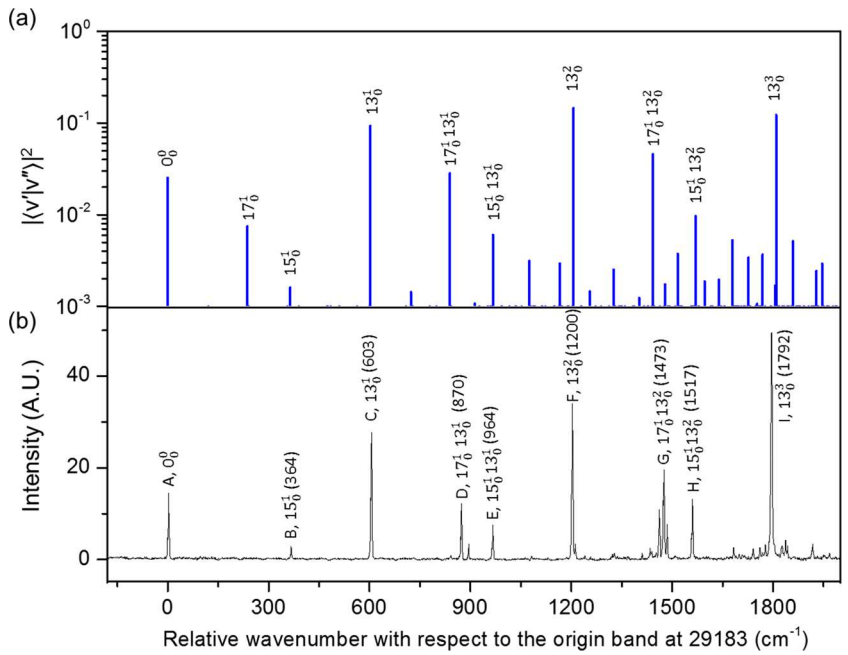

Figure 6. Comparison of the simulated (a) and the experimental (b) LIF spectra of the G conformer of the DFEO radical. Note that the computed values of ν_{15} and ν_{13} are scaled by 0.791 and 0.796, respectively, to match the experimental values (see text). Numbers in parentheses are transition frequencies relative to the origin band in cm^{-1}.

DOI: 10.1021/acs.jpca.9b09829
J. Phys. Chem. A 2019, 123, 10947−10960

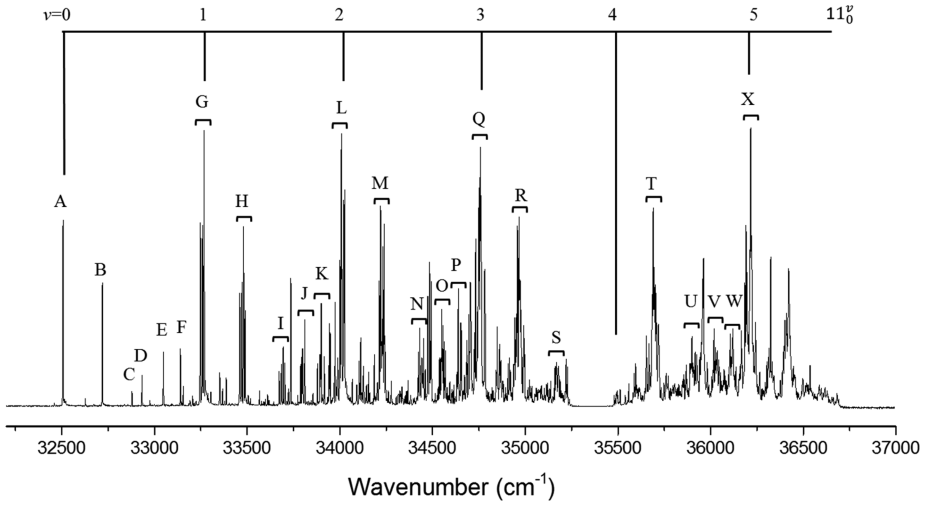

Figure 7. LIF spectrum of jet-cooled TFEO with the CO-stretch progression labeled.

Table 5. $\tilde{B} \leftarrow \tilde{X}$ Transition Frequencies and Vibrational Assignment of Strong Vibronic Bands Observed in the LIF Spectrum of TFEO[a]

label	expt freq (cm^{-1})	red shift (cm^{-1})	predicted freq (cm^{-1})	assignment	$\lvert\langle v'\rvert v''\rangle\rvert^2$
A	32506	0	0	0^0	0.03094
B	32719	213	217	17^1[b]	0.00364
C	32878	372	380	15^1[c]	0.00030
D	32933	427	435	17^2	0.00014
E	33048	542	544	13^1[d]	0.00093
F	33140	634	641	12^1[e]	0.00074
G	33262	756	794	11^1[f]	0.10882
H	33476	970	1012	$11^1 17^1$	0.01249
I	33689	1183	1175	$11^1 15^1$	0.00145
J	33802	1296	1339	$11^1 13^1$	0.00287
K	33898	1392	1437	$11^1 12^1$	0.00209
L	34014	1508	1590	11^2	0.17366
M	34227	1721	1807	$11^2 17^1$	0.0194
N	34437	1931	1970	$11^2 15^1$	0.00316
O	34553	2047	2133	$11^2 13^1$	0.00395
P	34644	2138	2231	$11^2 12^1$	0.00252
Q	34754	2248	2384	11^3	0.16513
R	34962	2456	2602	$11^3 17^1$	0.0179
S	35175	2669	2765	$11^3 15^1$	0.00405
			2929	$11^3 13^1$	0.00313
			3026	$11^3 12^1$	0.00165
			3180	11^4	0.10301
T	35693	3187	3396	$11^4 17^1$	0.01077
U	35909	3403	3559	$11^4 15^1$	0.0034
V	36031	3525	3723	$11^4 13^1$	0.00155
W	36113	3607	3821	$11^4 12^1$	0.00061
X	36210	3704	3975	11^5	0.04354

[a]Bands are labeled with Latin letters shown in Figure 6. [b]ν_{17}, OCC bending combined with CCF bending out-of-phase. [c]ν_{15}, OCC bending combined with CCF bending in-phase. [d]ν_{13}, CF_3 scissoring. [e]ν_{12}, CC stretch mixes with CF_3 ambarella. [f]ν_{11}, CO stretch.

according to the computations, the T conformer of MFEO has two vibrational modes that have large CO stretch character mixed with CF stretch and CC stretch, respectively. The fundamentals of these modes appear at 1041 and 1072 cm^{-1} in the experimental DF spectrum (see inset of Figure 9b), compared to 1075 and 1100 cm^{-1} from the computation. The discrepancy between the simulated and the experimental spectra in the high-frequency range in Figures 9−11 is mainly due to the anharmonicity. The simulated DF spectrum of the T conformer of DFEO, which is not observed experimentally, is presented in Figure S9 in comparison with that of the G conformer.

Computed and, if available, experimental $\tilde{X}$ state vibrational frequencies of the studied species, along with those of the $\tilde{B}$ state, are summarized in Tables S1−S5. For molecules belonging to the C_s point group, computed $\tilde{A}$ state vibrational frequencies (see Discussion) and the symmetries of vibrational modes (a' or a'') are also provided in the tables. Experimental harmonic frequencies (ω_e) and anharmonicity parameters ($\omega_e\chi_e$) of the CO-stretch mode of the studies species have been determined in fitting the Birge−Sponer plots (Figures S5−S8.) These values are summarized in Table S6.

DF spectra obtained by pumping CO-stretch bands in the LIF spectra are presented in the Supporting Information (Figures S10−S13). The similarity between DF spectra obtained by pump the origin band and the CO-stretch band of each conformer confirms the conformational assignment.

DISCUSSION

The comparison of experimentally determined spectroscopic parameters of ethoxy, MFEO, DFEO, and TFEO can help explore the most important structural and electronic effects in fluorinated ethoxy radicals. These parameters include the $\tilde{X}$ and $\tilde{B}$ state CO-stretch frequencies and the $\tilde{B} \leftarrow \tilde{X}$ excitation energies. The comparison between the experimental and simulated spectra serves as a good basis for testing the performance of the computational methods.

CO-Stretch Frequencies. The ethoxy radical and all three fluoroethoxy radicals studied in the present work have similar $\tilde{X}$ state CO-stretch frequencies ($\upsilon_{CO}^{\tilde{X}}$ between 1040 to 1080 cm^{-1}, see Table 2). This observation suggests that the fluorine atom(s) does not affect the CO bonding significantly in the ground electronic state, in which the 2pσ orbital of the CO bond is doubly occupied. The DFT-predicted values are very close to experimental ones, with scaling factors between 0.96 and 0.99.

The $\tilde{B}$ state CO-stretch frequencies ($\upsilon_{CO}^{\tilde{B}}$) of different fluorine substitutions and different conformers of the same molecule are not all close to each other. The G conformers of

DOI: 10.1021/acs.jpca.9b09829
J. Phys. Chem. A 2019, 123, 10947−10960

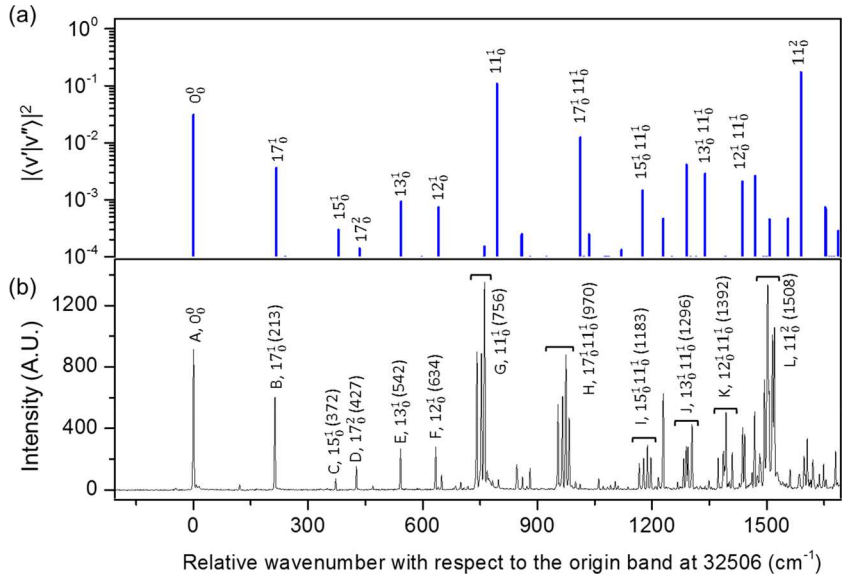

Figure 8. Comparison between the simulated (a) and experimental (b) LIF spectra of the TFEO radical. Frequencies of split vibronic bands are taken as averaged frequencies of the individual transitions weighted by their intensities (see text). Numbers in parentheses are transition frequencies relative to the origin band in cm^{-1}.

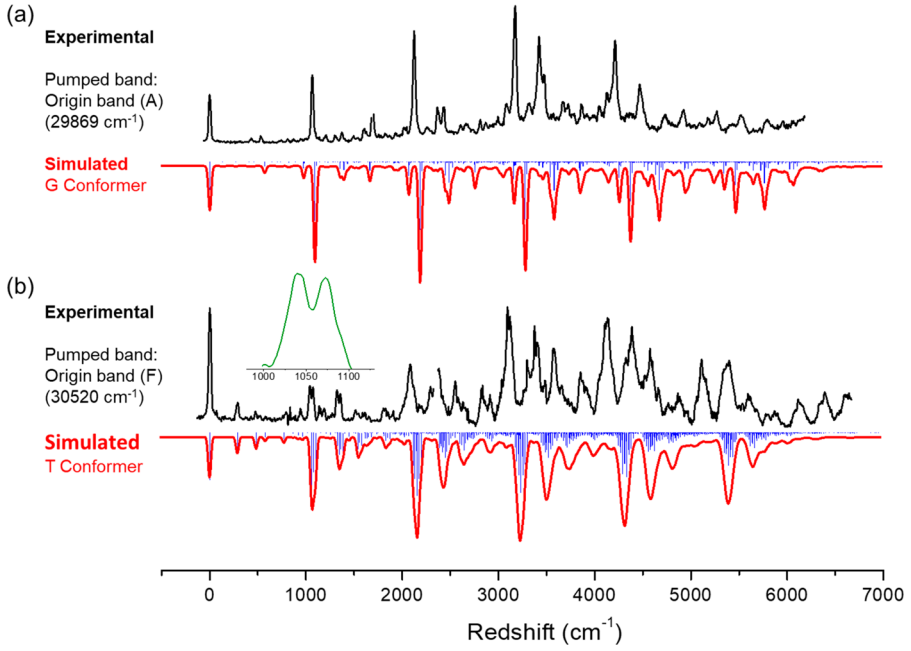

Figure 9. Comparison between the experimental (top, black trace) and simulated (bottom, red trace, inverted) DF spectra of the G conformer (a) and T conformer (b) of the MFEO radical. The experimental DF spectra were obtained by pumping the origin bands (A and F) of the two conformers in the LIF spectrum.

MFEO and DFEO have almost identical $\upsilon_{CO}^{\tilde{B}}$ as the ethoxy radical (603 cm^{-1}),[44] while those of the T conformer of MFEO (695 cm^{-1}) and the TFEO radical (756 cm^{-1}) are significantly larger. (The T conformer of DFEO was not experimentally detected.) In the $\tilde{B}$ state, the 2pσ orbital of the CO bond is singly occupied. Therefore, the CO bonding in the $\tilde{B}$ state is weaker than the ground state and more susceptible to substituent effects. For fluoroethoxy substituents, the possible substituent effects include[45,46] (a) the electric dipole field of the $-CH_xF_{3-x}$ group influencing the CO bond across space, that is, the *field effect*, and (b) the *α-inductive effect* transmitting from the fluorine atom(s) to the CO bond via successive polarization of the CF and the CC bonds. Both polar effects listed above could strengthen the CO bonding and increase the CO-stretch frequency. However, the conformational dependence of the CO-stretch frequency suggests that the polar effect is dominant through the field effect. This is not unexpected, because the inductive effect decreases exponentially down the CF and the CC bond. Therefore, it affects CO bonding insignificantly.

The conformational dependence of $\upsilon_{CO}^{\tilde{B}}$ can be explained as follows. The presence of electron-withdrawing groups (EWGs), in this case, the fluorine atoms, increases the acidity of adjacent hydrogens and, to a much smaller extent, the

DOI: 10.1021/acs.jpca.9b09829
J. Phys. Chem. A 2019, 123, 10947−10960

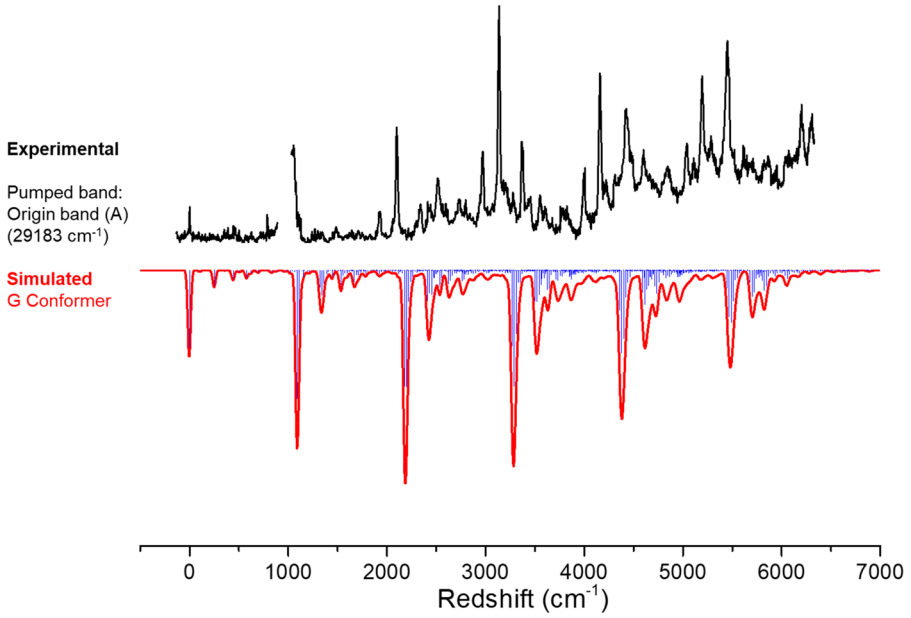

Figure 10. Comparison between the experimental (top, black trace) and simulated (bottom, red trace, inverted) DF spectra of the G conformer of the DFEO radical. The experimental DF spectra were obtained by pumping the origin band in the LIF spectrum (band A). The gap at ~1000 cm^{-1} is due to the scattering of the 355 nm photolysis laser.

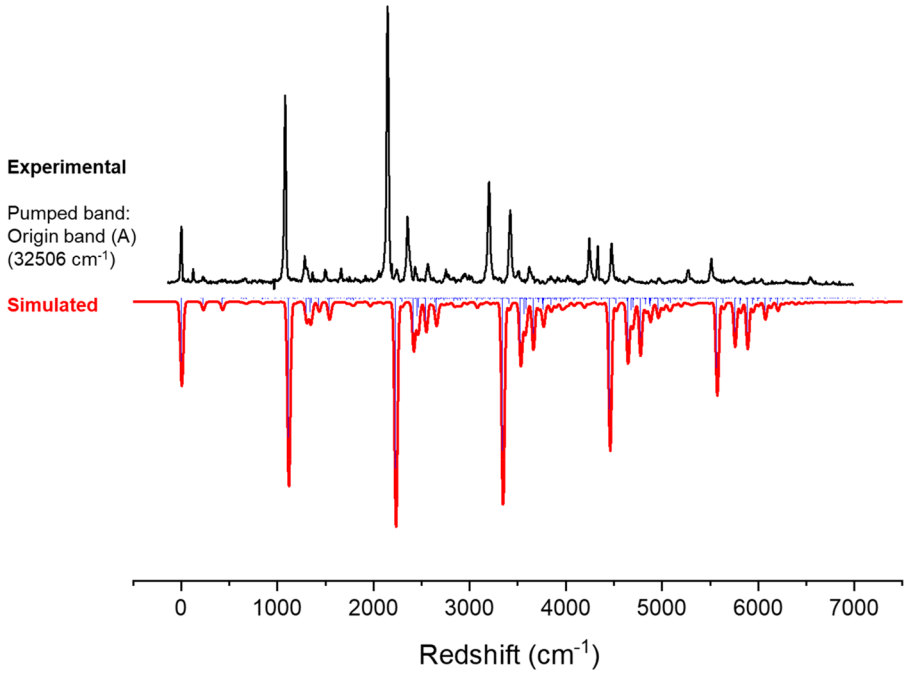

Figure 11. Comparison between the experimental (top, black trace) and simulated (bottom, red trace, inverted) DF spectra of TFEO radical. The experimental DF spectra were obtained by pumping the origin band in the LIF spectrum (band A).

hydrogens connected to the CO group. This inductive effect increases the positive charge on these hydrogens. Both the F and H atoms affect the CO bonding via the field effect, which strengthens and weakens the bond, respectively. For the G conformers of MFEO and DFEO, there are an F atom and an H atom at the *gauche* position (see Figure 1), which are closer to the CO bond than the H or F atom at the *trans* position. The experimental observation that the G conformers have almost identical $\tilde{\upsilon}^{B}_{CO}$ as ethoxy suggests that field effects of the negative charge on the F atom and the induced positive charge on the H atom largely cancel out in the G conformers.

Such long-range interactions need to be included in the computations to reproduce well the experimentally obtained spectra. Figures S14–S17 in the Supporting Information compare the experimental spectra and the simulated spectra using vibrational modes and frequencies computed by B3LYP and CAM-B3LYP method, using the same 6-311++G(d,p) basis set. Compared to B3LYP, CAM-B3LYP functional did a much better job of estimating vibrational frequencies of fluorinated ethoxy radicals, suggesting that it predicts this long-range interaction with a certain degree of accuracy. However, the CAM-B3LYP computation on the G conformer of DFEO

DOI: 10.1021/acs.jpca.9b09829
J. Phys. Chem. A 2019, 123, 10947−10960

overestimates its $\tilde{B}$-state CO-stretch frequency by ~26% (see Table 2). The exact reason for such a large discrepancy will require further detailed computational investigations (e.g., comparison of computations with different degrees of exchange interactions). It may be attributed to underestimation of the field effect of the induced positive charge on the H atom(s), which tends to weaken the singly occupied CO bond. Inspection of the Mulliken atomic charges reveals that the H atom at the β position of the G conformer of DFEO does have a larger induced positive charge than other fluorinated ethoxy radicals. (See Table S7 in the SI for Mulliken atomic charges.) Combined with the fact that this H atom in the G conformer is closer to the CO bond than the corresponding H atom in the T conformer of DFEO (see Figure 1), overestimation of $\upsilon_{CO}^{\tilde{B}}$ by the CAM-B3LYP calculation is not inconceivable.

$\tilde{B} \leftarrow \tilde{X}$ Excitation Energy. The adiabatic $\tilde{B} \leftarrow \tilde{X}$ excitation energy ($\Delta E^{\tilde{B}-\tilde{X}}$) of the G conformer of DFEO is almost the same as that of the ethoxy radical. $\Delta E^{\tilde{B}-\tilde{X}}$ of the two conformers of MFEO are slightly larger than ethoxy, whereas TFEO has a significantly larger $\Delta E^{\tilde{B}-\tilde{X}}$. Although a quantitative explanation is beyond the scope of the present work and not attempted, it is worth noting that the general trend of $\Delta E^{\tilde{B}-\tilde{X}}$ for different fluoroethoxy moieties and their conformers is the same as $\upsilon_{CO}^{\tilde{B}}$: Those with larger $\Delta E^{\tilde{B}-\tilde{X}}$ also have higher $\upsilon_{CO}^{\tilde{B}}$. (See Table 2). Therefore, the variation of $\Delta E^{\tilde{B}-\tilde{X}}$ may also be attributed to the field effect of F and H atoms in the $-CH_xF_{3-x}$ group.

In general, the CAM-B3LYP computations predict the $\tilde{B} \leftarrow \tilde{X}$ excitation energies of ethoxy and fluoroethoxy species quite well. For ethoxy, both conformers of MFEO and the TFEO radical, a consistent scaling factor of ~0.97 was determined by comparing to the experimental values. However, the discrepancy is significantly larger for the G conformer of DFEO (~11%). This is consistent with the fact that the CAM-B3LYP computations also significantly overestimate the B-state CO-stretch frequencies ($\upsilon_{CO}^{\tilde{B}}$) of this conformer (see above).

The $\tilde{A}$ States and $\tilde{A}-\tilde{X}$ Separations. In the DF spectra of MFEO, DFEO, and TFEO, all transitions can be reproduced by the simulated $\tilde{B} \rightarrow \tilde{X}$ spectra. No features in experimental DF spectra can be assigned to the $\tilde{B} \rightarrow \tilde{A}$ transition. This is different from primary and secondary alkoxy radicals,[26] as well as the CF_3O radical,[47] for which both $\tilde{B} \rightarrow \tilde{X}$ and $\tilde{B} \rightarrow \tilde{A}$ transitions were observed in DF spectra. In the present work, we resort to *ab initio* computations to predict the $\tilde{A}-\tilde{X}$ separation ($\Delta E^{\tilde{A}-\tilde{X}}$). $\Delta E^{\tilde{A}-\tilde{X}}$ of ethoxy, the T conformers of the MFEO and DFEO radicals, and TFEO, all of which belong to the C_s molecular point group, have been computed at the CAM-B3LYP/6-311++G(d,p) level of theory. The ethoxy radical was included as a control. For these molecules, the $\tilde{A}-\tilde{X}$ separation can be computed by promoting an electron from the $2p_x$ orbital to the half-filled $2p_y$ orbital of the O atom.[48,49] The computed $\tilde{A}-\tilde{X}$ separation of ethoxy (411 cm^{-1}) is close to the experimental values (see Table 2), benchmarking the computational method. The computed $\tilde{A}-\tilde{X}$ separations of fluoroethoxy species are all larger than 1000 cm^{-1}. For primary alkoxy radicals (other than methoxy), the $\tilde{A}-\tilde{X}$ separation is typically on the order of 100 cm^{-1}. Therefore, we attribute the $\tilde{B} \rightarrow \tilde{A}$ transition intensity to mixing between the $\tilde{A}$ and $\tilde{X}$ states. Consequently, the absence of the $\tilde{B} \rightarrow \tilde{A}$ transitions in the DF spectra of fluoroethoxy species can be rationalized by the large $\tilde{A}-\tilde{X}$ separations and hence less mixing between wave functions of these two electronic states.

The origin of the $\tilde{A}-\tilde{X}$ separation of alkoxy radicals has been discussed in detail in a recent paper by Liu.[49] In brief, it contains three contributions: the vibronic quenching, the difference between the zero-point energies of the two electronic states (ΔZPE), and the spin−orbit (SO) splitting. The effective SO constant ($a\zeta_e d$) of the ethoxy radical is −31.49(15) cm^{-1}.[44,50] For fluoroethoxies, $a\zeta_e d$ is expected to be smaller due to delocalization of the $2p_x$ and $2p_y$ orbitals of the O atom. ΔZPE values of alkoxy and fluorinated alkoxy radicals are also expected to be small because of the similarity between the potential energy surfaces (PESs) of the $\tilde{X}$ and $\tilde{A}$ states, which has been confirmed computationally.[48] Therefore, the relatively large $\tilde{A}-\tilde{X}$ separations of fluoroethoxy species are attributed to the larger vibronic quenching: the $-CH_xF_{3-x}$ group presents a barrier to the free orbital motion of the unpaired electron in the $2p_x$ (for the $\tilde{A}$ state) or $2p_y$ (the $\tilde{X}$ state) orbital due to Coulombic interactions. Such a hindering effect quenches the orbital angular momentum of the electron (**L**) and splits the two electronic states.[49,51]

The $-CH_xF_{3-x}$ Internal Rotation. In the experimental LIF spectrum of TFEO (Figures 7 and 8), vibronic bands of the CO-stretch mode and its combination bands are split due to the interaction between CO stretch and the $-CF_3$ internal rotation. Splitting of CO-stretch bands was also observed in the LIF spectra of *t*-butoxy[15] and secondary alkoxy radicals. We have carried out PES scans of ethoxy, MFEO, DFEO, and TFEO along the internal rotation coordinate, and the results are presented in the Supporting Information (see Figures S18−S21). The computations show that the internal rotation barrier of $-CF_3$ in $\tilde{B}$-state TFEO (1925 cm^{-1}) is more than 2 times higher than the $-CH_3$ internal rotation in $\tilde{B}$-state ethoxy (853 cm^{-1}). It is also significantly higher than that of the $\tilde{X}$-state TFEO (989 cm^{-1}). Barriers for internal rotations in MFEO and DFEO have also been determined by computations. Quantitative analysis of the $-CH_xF_{3-x}$ internal rotation and its interaction with CO stretch is deferred to a future publication.

Relative Energies of G and T Conformers. In the case of MFEO, the transitions of both T (lower-energy) and G (higher-energy) conformers are observed in the LIF spectra. In contrast to this, each band of the LIF spectrum of DFEO can be assigned to the G (lower-energy) conformer, and the higher-energy conformer (T) is not observed. (TFEO has only one conformer.) The presence of both conformers of MFEO and the absence of the T conformer of DFEO in the jet expansion can be rationalized by the larger energy difference between the two conformers of DFEO (computed ΔE = 100 cm^{-1}) compared to MFEO (ΔE = 586 cm^{-1}).

Computations suggest that the T conformer of the MFEO radical has lower energy than the G conformer, whereas for DFEO, the energy order is reversed: the G conformer has lower energy than T. Such results are supported by experimental observations (see above). Inspection of the molecular geometries (Figure 1) suggests that the difference in the energy orders is due to long-range interactions between the O atom and the β-position H atom(s) with an induced positive charge, which stabilizes the molecule.

CONCLUSIONS

The $\tilde{B}-\tilde{X}$ LIF and DF spectra of the $CH_xF_{3-x}CH_2O$ (x = 1, 2, 3) fluoroethoxy radicals (MFEO, DFEO, and TFEO) have been recorded under jet-cooled conditions. All stable conformers except the T conformer of DFEO are identified by simulating the spectra. The simulations use excitation energies,

DOI: 10.1021/acs.jpca.9b09829
J. Phys. Chem. A 2019, 123, 10947−10960

vibrational frequencies, and Franck−Condon factors computed at the CAM-B3LYP/6-311++G(d,p) level of theory. The $\tilde{B} \leftarrow \tilde{X}$ excitation energy ($\Delta E^{\tilde{B}-\tilde{X}}$) and the $\tilde{B}$ state CO-stretch frequency ($\upsilon_{CO}^{\tilde{B}}$) vary between different fluorine substitutions and different conformers of the same species. A comparison between the experimental and computed spectra suggests that the dominant substituent effect is the long-range field effect. Inclusion of such long-range interaction is critical to reproducing the experimentally obtained spectra of fluoroethoxy species. Such interactions can also be used to rationalize the relative large $\tilde{A}-\tilde{X}$ separations of fluoroethoxy species compared to the ethoxy radical and the relative energies of the T and G conformers of MFEO and DFEO. The vibronic bands of CO stretch and its combination bands are split due to interaction between the CO stretch mode and the $-CF_3$ internal rotation.

■ ASSOCIATED CONTENT

Supporting Information

The Supporting Information is available free of charge at https://pubs.acs.org/doi/10.1021/acs.jpca.9b09829.

Experimental and calculated frequencies, as well as symmetries, of vibrational modes, Mulliken atomic charges, determination of the harmonic frequencies (ω_e) and the anharmonic parameters ($\omega_e\chi_e$) of the CO-stretch mode by fitting Birge−Sponer plots, simulated DF spectra of T and G conformers of DFEO, comparison between the experimental spectra and spectra simulated using B3LYP and CAM-B3LYP calculations, and scans of PESs along the internal rotation coordinates (PDF)

■ AUTHOR INFORMATION

Corresponding Authors

*E-mail: j.liu@louisville.edu.

*E-mail: tarczay@chem.elte.hu.

ORCID

Jinjun Liu: 0000-0002-3968-2059

György Tarczay: 0000-0002-2345-1774

Present Address

‡G.B.: Wigner Research Centre for Physics, PO Box 32, H-1525 Budapest, Hungary.

Notes

The authors declare no competing financial interest.

■ ACKNOWLEDGMENTS

The authors are grateful to Prof. Terry A. Miller (Ohio State) for fruitful discussion. This work was supported by the Hungarian Scientific Research Fund (OTKA K108649), the ELTE Excellence Program (1783-3/2018/FEKUTSTRAT) supported by the Hungarian Ministry of Human Capacities (EMMI), and the National Science Foundation under Grant Number CHE-1454825.

■ REFERENCES

(1) Forster, P.; Ramaswamy, V.; Artaxo, P.; Berntsen, T.; Betts, R.; Fahey, D. W.; Haywood, J.; Lean, J.; Lowe, D. C.; Myhre, G. Changes in Atmospheric Constituents and in Radiative Forcing. In *Climate Change 2007. The Physical Science Basis*; Solomon, S., Miller, H. L., Tignor, M., Averyt, K. B., Marquis, M., Chen, Z., Manning, M., Qin, D., Eds.; Cambridge University Press: Cambridge, United Kingdom, and New York, NY, USA, 2007; Chapter 2.

(2) Atkinson, R. Gas-Phase Tropospheric Chemistry of Organic Compounds. *J. Phys. Chem. Ref. Data* 1989, Monograph No. 1.

(3) Derwent, R.; Volz-Thomas, A.; Prather, M. *World Meteorological Organization Global Ozone Research and Monitoring Project*; Report.

(4) Carter, C. C.; Atwell, J. R.; Gopalakrishnan, S.; Miller, T. A. Jet-Cooled Laser-Induced Fluorescence Spectroscopy of Some Alkoxy Radicals. *J. Phys. Chem. A* **2000**, *104*, 9165−9170.

(5) Nielsen, O. J.; Gamborg, E.; Sehested, J.; Wallington, T. J.; Hurley, M. D. Atmospheric Chemistry of HFC-143a: Spectrokinetic Investigation of the $CF_3CH_2O_2\cdot$ Radical, Its Reactions with NO and NO2, and the Fate of $CF3_CH2_O$. *J. Phys. Chem.* **1994**, *98*, 9518−9525.

(6) Carter, C. C.; Gopalakrishnan, S.; Atwell, J. R.; Miller, T. A. Laser Excitation Spectra of Large Alkoxy Radicals Containing 5− 12 Carbon Atoms. *J. Phys. Chem. A* **2001**, *105*, 2925−2928.

(7) Chhantyal-Pun, R.; Roudjane, M.; Melnik, D. G.; Miller, T. A.; Liu, J. Jet-Cooled Laser-Induced Fluorescence Spectroscopy of Isopropoxy Radical: Vibronic Analysis of $\tilde{B}-\tilde{X}$ and $\tilde{B}-\tilde{A}$ Band Systems. *J. Phys. Chem. A* **2014**, *118*, 11852−11870.

(8) Gopalakrishnan, S.; Carter, C. C.; Zu, L.; Stakhursky, V.; Tarczay, G.; Miller, T. A. Rotationally Resolved $\tilde{B}-\tilde{X}$ Electronic Spectra of Both Conformers of the 1-Propoxy Radical. *J. Chem. Phys.* **2003**, *118*, 4954−4969.

(9) Gopalakrishnan, S.; Zu, L.; Miller, T. A. Rotationally Resolved Electronic Spectra of the $\tilde{B}-\tilde{X}$ Transition in Multiple Conformers of 1-Butoxy and 1-Pentoxy Radicals. *J. Phys. Chem. A* **2003**, *107*, 5189−5201.

(10) Hao, H.; Wang, L.; Zu, L. Methyl Substitution Effect on the Jet-Cooled Laser-Induced Fluorescence Spectrum of Cyclohexoxy Radical. *J. Phys. Chem. A* **2015**, *119*, 3384−3392.

(11) Liang, G.; Liu, C.; Hao, H.; Zu, L.; Fang, W. Laser-Induced Fluorescence of Isobutoxy in Competition with Ground State Decomposition. *J. Phys. Chem. A* **2013**, *117*, 13229−13235.

(12) Lin, J.; Wu, Q.; Liang, G.; Zu, L.; Fang, W. Jet-Cooled Laser-Induced Fluorescence Spectroscopy of Methylcyclohexoxy Radicals. *RSC Adv.* **2012**, *2*, 583−589.

(13) Lin, J.; Zu, L.; Fang, W. Conformation and Spectroscopy Study of Cycloheptoxy Radical. *J. Phys. Chem. A* **2011**, *115*, 274−279.

(14) Liu, J.; Miller, T. A. Jet-Cooled Laser-Induced Fluorescence Spectroscopy of Cyclohexoxy: Rotational and Fine Structure of Molecules in Nearly Degenerate Electronic States. *J. Phys. Chem. A* **2014**, *118*, 11871−11890.

(15) Liu, J.; Reilly, N. J.; Mason, A.; Miller, T. A. Laser-Induced Fluorescence Spectroscopy of Jet-Cooled t-Butoxy. *J. Phys. Chem. A* **2015**, *119*, 11804−11812.

(16) Reza, M. A.; Paul, A. C.; Reilly, N. J.; Liu, J. Laser-Induced Fluorescence and Dispersed Fluorescence Spectroscopy of Jet-Cooled Isopentoxy Radicals. *J. Phys. Chem. A* **2019**, *123*, 8441.

(17) Stakhursky, V. L.; Zu, L.; Liu, J.; Miller, T. A. High Resolution Spectra and Conformational Analysis of 2-Butoxy Radical. *J. Chem. Phys.* **2006**, *125*, 094316.

(18) Wang, C.; Deng, W.; Shemesh, L. G.; Lilien, M. D.; Katz, D. R.; Dibble, T. S. Observation of Fluorescence Excitation Spectra of tert-Pentoxy and 3-Pentoxy Radicals. *J. Phys. Chem. A* **2000**, *104*, 10368−10373.

(19) Wang, C.; Shemesh, L. G.; Deng, W.; Lilien, M. D.; Dibble, T. S. Laser-Induced Fluorescence Excitation Spectra of tert-Butoxy and 2-Butoxy Radicals. *J. Phys. Chem. A* **1999**, *103*, 8207−8212.

(20) Zhang, L.; Callahan, K. M.; Derbyshire, D.; Dibble, T. S. Laser-Induced Fluorescence Spectra of 4-Methylcyclohexoxy Radical and Perdeuterated Cyclohexoxy Radical and Direct Kinetic Studies of Their Reactions with O_2. *J. Phys. Chem. A* **2005**, *109*, 9232−9240.

(21) Zu, L.; Liu, J.; Gopalakrishnan, S.; Miller, T. A. The Rotationally Resolved Electronic Spectra of Several Conformers of 1-Hexoxy and 1-Heptoxy. *Can. J. Chem.* **2004**, *82*, 854−866.

(22) Zu, L.; Liu, J.; Tarczay, G.; Dupré, P.; Miller, T. A. Jet-Cooled Laser Spectroscopy of the Cyclohexoxy Radical. *J. Chem. Phys.* **2004**, *120*, 10579−10593.

DOI: 10.1021/acs.jpca.9b09829
J. Phys. Chem. A 2019, 123, 10947−10960

(23) Wu, Q.; Liang, G.; Zu, L.; Fang, W. Vibrationally Resolved LIF Spectrum of Tertiary Methylcyclohexoxy Radical. *J. Phys. Chem. A* **2012**, *116*, 3156−3162.
(24) Paul, A. C.; Sharma, K.; Reza, M. A.; Telfah, H.; Miller, T. A.; Liu, J. Laser-Induced Fluorescence and Dispersed-Fluorescence Spectroscopy of the $\tilde{A}^2E-\tilde{X}^2A_1$ Transition of Jet-Cooled Calcium Methoxide ($CaOCH_3$) Radicals. *J. Chem. Phys.* **2019**, *151*, 134303.
(25) Alam, J.; Reza, M. A.; Mason, A.; Reilly, N. J.; Liu, J. Dispersed Fluorescence Spectroscopy of Jet-Cooled 2-, 3-, and 4-Methylcyclohexoxy Radicals. *J. Phys. Chem. A* **2015**, *119*, 6257−6268.
(26) Jin, J.; Sioutis, I.; Tarczay, G.; Gopalakrishnan, S.; Bezant, A.; Miller, T. A. Dispersed Fluorescence Spectroscopy of Primary and Secondary Alkoxy Radicals. *J. Chem. Phys.* **2004**, *121*, 11780−11797.
(27) Reza, M. A.; Paul, A. C.; Reilly, N. J.; Alam, J.; Liu, J. Dispersed Fluorescence Spectroscopy of Jet-Cooled Isobutoxy and 2-Methyl-1-Butoxy Radicals. *J. Phys. Chem. A* **2016**, *120*, 6761−6767.
(28) Paul, A. C.; Reza, M. A.; Liu, J. Dispersed-Fluorescence Spectroscopy of Jet-Cooled Calcium Ethoxide Radical ($CaOC_2H_5$). *J. Mol. Spectrosc.* **2016**, *330*, 142−146.
(29) Liu, J.; Chen, M.-W.; Melnik, D.; Yi, J. T.; Miller, T. A. The Spectroscopic Characterization of the Methoxy Radical. I. Rotationally Resolved $\tilde{A}\ ^2A_1$- $\tilde{X}\ E_2$ Electronic Spectra of CH_3O. *J. Chem. Phys.* **2009**, *130*, 074302.
(30) Melnik, D. G.; Liu, J.; Chen, M.-W.; Miller, T. A.; Curl, R. F. The Spectroscopic Characterization of the Methoxy Radical. III. Rotationally Resolved $\tilde{A}\ ^2A_1$- $\tilde{X}\ E_2$ Electronic and $\tilde{X}\ E_2$ Submillimeter Wave Spectra of Partially Deuterated CH_2DO and CHD_2O Radicals. *J. Chem. Phys.* **2011**, *135*, 094310.
(31) Liu, J.; Chen, M.-W.; Melnik, D.; Miller, T. A.; Endo, Y.; Hirota, E. The Spectroscopic Characterization of the Methoxy Radical. II. Rotationally Resolved $\tilde{A}^2A_1$- $\tilde{X}E_2$ Electronic and $\tilde{X}E_2$ Microwave Spectra of the Perdeuteromethoxy Radical CD_3O. *J. Chem. Phys.* **2009**, *130*, 074303.
(32) Chhantyal-Pun, R.; Chen, M.-W.; Sun, D.; Miller, T. A. Detection and Characterization of Products from Photodissociation of XCH_2CH_2ONO (X= F, Cl, Br, OH). *J. Phys. Chem. A* **2012**, *116*, 12032−12040.
(33) Li, Z.; Francisco, J. Laser-Induced Fluorescence Spectroscopic Study of the $\tilde{A}^2A_1-\tilde{X}\ ^2E$ Transition of Trifluoromethoxy Radical. *Chem. Phys. Lett.* **1991**, *186*, 336−342.
(34) Chhantyal-Pun, R.; Chen, M.-W.; Miller, T. A. Laser-Induced Fluorescence Study of the $\tilde{B}-\tilde{X}$ Transition of FCH_2CH_2O. *Chem. Phys. Lett.* **2013**, *555*, 64−71.
(35) Furubayashi, M.; Bridier, I.; Inomata, S.; Washida, N.; Yamashita, K. Laser-Induced Fluorescence of the CH_2CFO Radical. *J. Chem. Phys.* **1997**, *106*, 6302−6309.
(36) Inomata, S.; Furubayashi, M.; Imamura, T.; Washida, N.; Yamaguchi, M. Laser-Induced Fluorescence of the CD_2CFO Radical. *J. Chem. Phys.* **1999**, *111*, 6356−6362.
(37) Wright, S. A.; Dagdigian, P. J. Rotational Analysis of the $\tilde{B}^2A''-\tilde{X}^2A''$ Origin Band of the CH_2CFO radical. *J. Chem. Phys.* **1997**, *107*, 9755−9758.
(38) Yamaguchi, M.; Furubayashi, M.; Inomata, S.; Washida, N. Analysis of Laser-Induced Fluorescence Spectra of the $\tilde{B}\ ^2A''-\tilde{X}\ ^2A''$ Transition With Calculated Franck−Condon Factors of CH_2CFO. *Chem. Phys. Lett.* **1998**, *298*, 93−100.
(39) Inomata, S.; Yamaguchi, M.; Washida, N. Laser-induced fluorescence of the CHXCFO (X= F, Cl) radicals. *J. Chem. Phys.* **2002**, *116*, 6961−6972.
(40) Shuping, L.; Chwee, T. S.; Fan, W. Y. FTIR Studies on the Gas Phase Laser-Induced Decomposition of CF_3CH_2ONO. *Chem. Phys.* **2006**, *320*, 259−266.
(41) Yanai, T.; Tew, D. P.; Handy, N. C. A New Hybrid Exchange−Correlation Functional Using the Coulomb-Attenuating Method (CAM-B3LYP). *Chem. Phys. Lett.* **2004**, *393*, 51−57.
(42) Frisch, M. J.; Trucks, G. W.; Schlegel, H. B.; Scuseria, G. E.; Robb, M. A.; Cheeseman, J. R.; Scalmani, G.; Barone, V.; Mennucci, B.; Petersson, G. A.; Nakatsuji, H.; Caricato, M.; Li, X.; Hratchian, H. P.; Izmaylov, A. F.; Bloino, J.; Zheng, G.; Sonnenberg, J. L.; Hada, M.; Ehara, M.; Toyota, K.; Fukuda, R.; Hasegawa, J.; Ishida, M.; Nakajima, T.; Honda, Y.; Kitao, O.; Nakai, H.; Vreven, T.; Montgomery, J. A., Jr.; Peralta, J. E.; Ogliaro, F.; Bearpark, M.; Heyd, J. J.; Brothers, E.; Kudin, K. N.; Staroverov, V. N.; Kobayashi, R.; Normand, J.; Raghavachari, K.; Rendell, A.; Burant, J. C.; Iyengar, S. S.; Tomasi, J.; Cossi, M.; Rega, N.; Millam, J. M.; Klene, M.; Knox, J. E.; Cross, J. B.; Bakken, V.; Adamo, C.; Jaramillo, J.; Gomperts, R.; Stratmann, R. E.; Yazyev, O.; Austin, A. J.; Cammi, R.; Pomelli, C.; Ochterski, J. W.; Martin, R. L.; Morokuma, K.; Zakrzewski, V. G.; Voth, G. A.; Salvador, P.; Dannenberg, J. J.; Dapprich, S.; Daniels, A. D.; Farkas, O.; Foresman, J. B.; Ortiz, J. V.; Cioslowski, J.; Fox, D. J. *Gaussian 09*, revision C.01; Gaussian, Inc.: Wallingford, CT, 2009.
(43) Mozhayskiy, V.; Krylov, A. *ezSpectrum*, version 3.0., University of Southern California, Los Angeles, http://iopenshell.usc.edu, 2008.
(44) Tan, X. Q.; Williamson, J. M.; Foster, S. C.; Miller, T. A. Rotationally Resolved Electronic Excitation Spectra of the Ethoxy $\tilde{B} \leftarrow \tilde{X}$ Transition. *J. Phys. Chem.* **1993**, *97*, 9311−9316.
(45) Dewar, M. J. S.; Grisdale, P. J. Substituent Effects. I. Introduction. *J. Am. Chem. Soc.* **1962**, *84*, 3539−3541.
(46) Stock, L. M. The Origin of the Inductive Effect. *J. Chem. Educ.* **1972**, *49*, 400.
(47) Tan, X.-Q.; Yang, M.-C.; Carter, C. C.; Williamson, J. M.; Miller, T. A.; Mlsna, T. E.; Anderson, J. D. O.; Desmarteau, D. D. Electronic Spectroscopy of CF_3O in a Supersonic Jet: Symmetry and Rotational Structure of a Prototypical Perfluoroalkoxy Radical. *J. Phys. Chem.* **1994**, *98*, 2732−2734.
(48) Liu, J.; Melnik, D.; Miller, T. A. Rotationally Resolved $\tilde{B}\leftarrow\tilde{X}$ Electronic Spectra of the Isopropoxy Radical: A Comparative Study. *J. Chem. Phys.* **2013**, *139*, 094308.
(49) Liu, J. Rotational and fine structure of open-shell molecules in nearly degenerate electronic states. *J. Chem. Phys.* **2018**, *148*, 124112.
(50) Yan, Y.; Miller, T. A.; Liu, J. Analyzing the rotational and spin structure of the two lowest electronic states of asymmetrically substituted alkoxy radicals. Presented at the 74th International Symposium on Molecular Spectroscopy, Champaign-Urbana, IL, 2019.
(51) Mills, P. D. A.; Western, C. M.; Howard, B. J. Rotational spectra of rare gas-nitric oxide van der Waals molecules. Part 1. Theory of the rotational energy levels. *J. Phys. Chem.* **1986**, *90*, 3331−3338.
(52) Zhu, X.; Kamal, M. M.; Misra, P. Laser-Induced Excitation and Dispersed Fluorescence Spectra of the Ethoxy Radical. *Pure Appl. Opt.* **1996**, *5*, 1021−1029.
(53) Ramond, T. M.; Davico, G. E.; Schwartz, R. L.; Lineberger, W. C. Vibronic Structure of Alkoxy Radicals via Photoelectron Spectroscopy. *J. Chem. Phys.* **2000**, *112*, 1158−1169.

DOI: 10.1021/acs.jpca.9b09829
J. Phys. Chem. A 2019, 123, 10947−10960